1674 *Inorg. Chem.* **2010**, *49*, 1674–1678
DOI: 10.1021/ic902081r

Inorganic Chemistry
Article

Facile Synthesis and Luminescence of $Sr_5(PO_4)_3Cl:Eu^{2+}$ Nanorod Bundles via a Hydrothermal Route

Yanhua Song, Hongpeng You,* Mei Yang, Yuhua Zheng, Kai Liu, Guang Jia, Yeju Huang, Lihui Zhang, and Hongjie Zhang*

State key Laboratory of Rare Earth Resource Utilization, Changchun Institute of Applied Chemistry, Chinese Academy of Sciences, 130022, P.R. China and Graduate University of the Chinese Academy of Sciences, Beijing 100049, P.R. China

Received October 21, 2009

$Sr_5(PO_4)_3Cl:Eu^{2+}$ nanorod bundles were successfully prepared through a facile hydrothermal method. The X-ray diffraction (XRD) and FT-IR results demonstrate that the product is a pure hexagonal phase of $Sr_5(PO_4)_3Cl$. The scanning electron microscopy (SEM), transmission electron microscopy (TEM), and high-resolution TEM (HRTEM) images indicate that the as-prepared $Sr_5(PO_4)_3Cl:Eu^{2+}$ nanorod bundles consist of parallel nanorods with diameters ranging from 20 to 30 nm and that the nanorods grow along the [002] direction. The photoluminescence spectra show that the Eu^{3+} ions have been reduced to Eu^{2+} ions successfully and that the as-obtained $Sr_5(PO_4)_3Cl:Eu^{2+}$ phosphor exhibited intense blue emission. Furthermore, this new simple synthetic route may be of much significance in the synthesis of other divalent europium ions activated nanoscale phosphors by aqueous method.

Introduction

In past 10 years, nanomaterials have attracted considerable attention because of their unique physical properties and promising potential applications in various fields such as optics, electronics, catalysis, biotechnology, and ceramics.[1−3] Among the various nanomaterials, nanophosphors containing rare earth ions have been particularly attractive from both a fundamental and a practical viewpoint mainly because of their unique luminescent properties coming from the intra 4f transitions of the trivalent rare earth ions, such as Pr^{3+}, Eu^{3+}, Tb^{3+}, Sm^{3+}, Er^{3+}, and so on.[4] However, the nanophosphors containing rare earth ions that involve the transitions between the $4f^n$ and $4f^{n-1}5d$ levels of Eu^{2+} and Yb^{2+} ions have been paid little attention although they can emit strong light in the range from UV to red which is of significance in various applications. One of the main reasons is that the formation of nanophosphors usually needs a low temperature solution process, while the formation of the phosphor containing Eu^{2+} ions requires a high temperature reduction process because the europium is often in the form of Eu^{3+} ion in solution and lacks an efficient reduction mechanism in solution. Therefore, the synthesis of nanophosphors containing Eu^{2+} ions is still a challenge to material scientists. In addition, among highly efficient tricolor luminescent materials for lamps or cathode phosphors, red and green nanophosphors have been widely reported, while blue nanophosphors are limited. To realize white light in the field of advanced optoelectronic and microelectronic devices, it is necessary to develop highly efficient blue nanophosphors.

Alkaline-earth-metal halophosphates have the generic molecular formula $M_5(PO_4)_3X$ (M = Ca, Sr, Ba; X = F, Cl, Br, OH) and are well-known for their applications as luminescent materials,[5] laser hosts,[6] and biocompatible materials.[7] One of the well-known apatites is $Sr_5(PO_4)_3Cl:Eu^{2+}$. It is a highly efficient luminescent material, used as the blue component in high-efficiency compact fluorescent lamps, white LEDs, and backlight for desktop monitors and LCD TVs because of its low price, environmental friendliness, good thermal stability, and high quantum efficiency.[8] Therefore, various synthesis techniques have been developed for the preparation of chloroapatite, including traditional high temperature solid state reaction,[9] self-propagating high-temperature synthesis,[10]

*To whom correspondence should be addressed. E-mail: hpyou@ciac.jl.cn (H.Y.), hongjie@ciac.jl.cn (H.Z.).

(1) Thiaville, A.; Miltat, J. *Science* **1991**, *284*, 1939.
(2) Xia, Y. N.; Yang, P. D.; Sun, Y. G.; Wu, Y. Y.; Mayers, B.; Gates, B.; Yin, Y. D.; Kim, F. L.; Yan, H. Q. *Adv. Mater.* **2003**, *15*, 353.
(3) Fang, X. P.; Xu, A. W.; You, L. P.; Song, R. Q.; Yu, J. C.; Zhang, H. X.; Li, Q.; Liu, H. Q. *Adv. Funct. Mater.* **2003**, *13*, 955.
(4) Zhang, X.; Zhang, J.; Nie, Z.; Wang, M.; Ren, X.; Wang, X. *Appl. Phys. Lett.* **2007**, *90*, 151911. Jia, G.; You, H.; Song, Y.; Jia, J.; Zheng, Y.; Zhang, L.; Liu, K.; Zhang, H. *Inorg. Chem.* **2009**, *48*, 10193. Yu, M.; Lin, J.; Wang, Z.; Fu, J.; Wang, S.; Zhang, H. J.; Han, Y. C. *Chem. Mater.* **2002**, *14*, 2224. Boyer, J. C.; Vetrone, F.; Cuccia, L. A.; Capobianco, J. A. *J. Am. Chem. Soc.* **2006**, *128*, 7444.
(5) Feldmann, C.; Jüstel, T.; Ronda, C. R.; Schmidt, P. J. *Adv. Funct. Mater.* **2003**, *13*, 511.
(6) Budin, J. B.; Michael, J. C.; Auzel, F. *J. Appl. Phys.* **1979**, *50*, 641.
(7) Wang, X.; Zhuang, J.; Peng, Q.; Li, Y. D. *Adv. Mater.* **2006**, *18*, 2031.
(8) Welker, T. *J. Lumin.* **1991**, *48−49*, 49.
(9) Pallila, F. C.; O'Reilly, B. E. *J. Electrochem. Soc.* **1968**, *115*, 1076.
(10) Kottaisamy, M.; Rao, M. M.; Jeyakumar, D. *J. Mater. Chem.* **1997**, *7*, 345.

 Published on Web 01/07/2010

spray pyrolysis technique,[11] precipitation route,[12] and aqueous colloidal method.[13] Among these methods, the high temperature solid state processes are usually used and can easily reduce the Eu^{3+} ions to Eu^{2+} ions. But the resulting particles are about 10 μm in size, irregular in shape, and sometimes sintered into large aggregates, which are not suitable for nanoscale electronic or optoelectronic devices. Spray pyrolysis technique can obtain the spherical phosphor containing Eu^{2+} ions. Nevertheless, particle size is limited to submicrometer size. Although the aqueous process can obtain nanoparticles, the OH^- contamination could not be avoided, leading to the formation of $M_5(PO_4)_3Cl_{1-x}(OH)_x$, which greatly decrease luminescent quantum efficiency. Therefore, it would be desirable to find a mild process for production of high purity Eu^{2+}-activated chloroapatite nanophosphors which could be suitable for use in nanoscale electronic or optoelectronic devices.

As an important technique for inorganic materials synthesis, the hydrothermal process has been widely used in recent years to prepare nanomaterials with uniform size.[14,15] However, no report focuses on the synthesis of $Sr_5(PO_4)_3Cl:Eu^{2+}$ blue phosphor by the hydrothermal route. Hydrothermal synthesis of $Sr_5(PO_4)_3Cl:Eu^{2+}$ has two challenges. One is the reduction of the Eu^{3+} ions at low temperature in solution since the Eu^{2+}-activated phosphors usually are synthesized at high temperature (~1000 °C) and under a reduction atmosphere.[16] In solution, europium ions usually exist as trivalent ions. There is rarely a report on the reduction from the Eu^{3+} to Eu^{2+} ions by aqueous methods. The other challenge is the hydroxyl ion (OH^-) contamination. The chloro- and hydroxyapatites crystallize under a hexagonal system with very close crystallographic cell parameters.[17] So chloroapatites could crystallize accompanied with the hydroxyapatites. Up to now, hydrothermal synthesis has not yielded high-purity Eu^{2+}-doped chloroapatite.

Herein, we report the synthesis of $Sr_5(PO_4)_3Cl:Eu^{2+}$ blue nanophosphors with high purity one-dimensional nanorods and nanorod bundles through a facile and mild hydrothermal process. The reduction of europium ions were realized by $N_2H_4 \cdot H_2O$ in solution for the first time. The optical properties of the $Sr_5(PO_4)_3Cl:Eu^{2+}$ nanophosphors were also investigated. The simplicity of the synthetic route makes it promising for the preparation to other divalent europium-activated phosphors in solution.

Experimental Section

Preparation. Eu_2O_3 (99.99%) was purchased from Shanghai Yuelong Non-Ferrous Metals Limited. The other chemicals were purchased from Beijing Chemical Co., and all chemicals are analytical grade reagents and used directly without further purification. $Eu(NO_3)_3$(0.05 M) stock solution was prepared by dissolving the corresponding Eu_2O_3 in nitric acid at elevated temperature.

In a typical procedure, 0.24 mmol $SrCl_2$ was first dissolved into 1 mL of water in Teflon linear by ultrasonic. Twenty-five milliliters of ethanol with 0.2 mmol $Eu(NO_3)_3$ was then added into the solution under stirring. Thereafter, ethylenediamine tetraacetic acid (EDTA) (0−0.5 g) and $N_2H_4 \cdot H_2O$ (> 50%) (0−4 mL) were introduced into the above solution in sequence. Afterward, a solution of H_3PO_4 (0.1 mL, 85%) in 10 mL of anhydrous ethanol was added dropwise. After vigorous stirring for 30 min, the linear was put into the autoclave, and the suspension was degassed with the N_2-H_2 (V/V = 9/1) for 30 min. All the above experiments are operated in the fume cupboard. The autoclave was finally maintained in an electric oven at 180 °C for 24 h. After naturally cooling to room temperature, the resulting white powder product was carefully collected by centrifugation (6000 g/min) and washed several times with deionic water and absolute ethanol. The final product was dried in air at 60 °C for 12 h. The bulk $Sr_5(PO_4)_3Cl:Eu^{2+}$ was obtained by a direct solid state reaction using stoichiometric amounts of $SrCO_3$, $(NH_4)_2HPO_4$, $SrCl_2 \cdot 6H_2O$ (50% excess), and Eu_2O_3 at 1000 °C for 2 h under a CO reducing atmosphere.

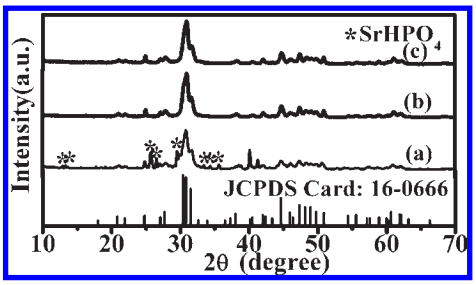

Figure 1. XRD patterns of the nanocrystalline chloroapatite samples prepared at 180 °C for 24 h with different ratio of $Sr(NO_3)_2$ to $SrCl_2$. (a) $Sr(NO_3)_2/SrCl_2$ = 4.5:0.5; (b) $Sr(NO_3)_2/SrCl_2$ = 1:1; (c) $Sr(NO_3)_2/SrCl_2$ = 0:5.

Characterization. The X-ray diffraction (XRD) patterns of the samples were carried out on a Rigaku-Dmax 2500 diffractometer using Cu Kα radiation (λ = 0.15405 nm). Fourier transform infrared spectroscopy (FT-IR) spectra were performed on Perkin-Elmer 580B infrared spectrophotometer using the KBr pellet technique. The morphology and energy dispersive X-ray spectra (EDS) were examined using a field emission scanning electron microscope (FE-SEM, S-4800 Hitachi Corp., Tokyo). Low- and high-resolution transmission electron microscopy (TEM) was obtained using a JEOL JEM-2100F microscope operating at an accelerating voltage of 200 kV. The excitation and emission spectra were performed on a Hitachi F-4500 spectrophotometer equipped with a 150 W xenon lamp as the excitation source. All the measurements were performed at room temperature.

Results and Discussion

Phase Formation. The product synthesized by the hydrothermal method was affected by the quantity of Cl^- ions in raw materials. Figure1 shows the XRD patterns of the nanocrystalline chloroapatite samples prepared at 180 °C for 24 h with different ratio of $Sr(NO_3)_2$ to $SrCl_2$. When the mole ratio of $Sr(NO_3)_2$ to $SrCl_2$ equaled 4.5:0.5, which matches well with the mole ratio of Sr^{2+} to Cl^- in the formula, not only the $Sr_5(PO_4)_3Cl:Eu^{2+}$ phase but also the $SrHPO_4$ phase could be observed. When the mole ratio equals 1:1 or 0:5, which means the Cl^- ions excess the theoretic amount, all the diffraction peaks of the samples can be assigned exactly to the standard data of $Sr_5(PO_4)_3Cl:Eu^{2+}$. No second phase was detected. According to the EDS data (Figure 2), the ratios of Sr^{2+} to Cl^- were 30.29/5.83 and 30.61/5.98, which were near to the theoretic ratio 5:1. For the following discussions, the mole ratio of $Sr(NO_3)_2$ to $SrCl_2$ was fixed at 0:5.

(11) Wang, W. N.; Iskandar, F.; Okuyama, K; Shinomiya, Y. *Adv. Mater.* **2008**, *20*, 3422.
(12) Layrolle, P.; Lebugle, A. *Chem. Mater.* **1996**, *8*, 134.
(13) Ramesh, R.; Jagannathan, R. *J. Phys. Chem. B* **2000**, *104*, 8351.
(14) Wang, L. Y.; Li, P.; Li, Y. D. *Adv. Mater.* **2007**, *19*, 3304.
(15) Shi, W.; Zhou, L.; Song, S.; Yang, J.; Zhang, H. *Adv. Mater.* **2008**, *20*, 1892.
(16) Nötzold, D.; Wulff, H. *Phys. Status Solidi B* **1998**, *207*, 271.
(17) Ropp, R. C. *Studies in inorganic chemistry 12: Luminescence and the solid state*; Elsevier: Amsterdam, 1991; Chapter 10.

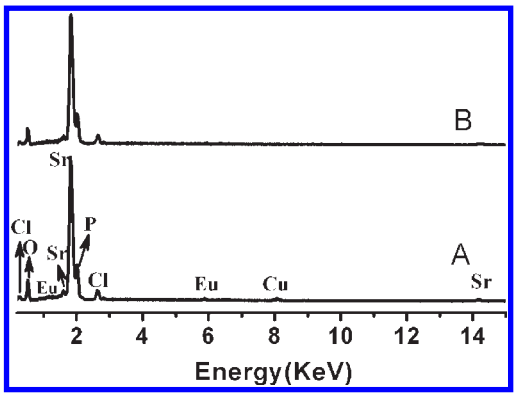

Figure 2. EDS patterns of samples synthesized with different ratio of $Sr(NO_3)_2$ to $SrCl_2$. Both of the samples were hydrothermal treated at 180 °C for 24 h with 0.50 g EDTA. (A) $Sr(NO_3)_2/SrCl_2$ = 0:5; (B) $Sr(NO_3)_2/SrCl_2$ = 1:1.

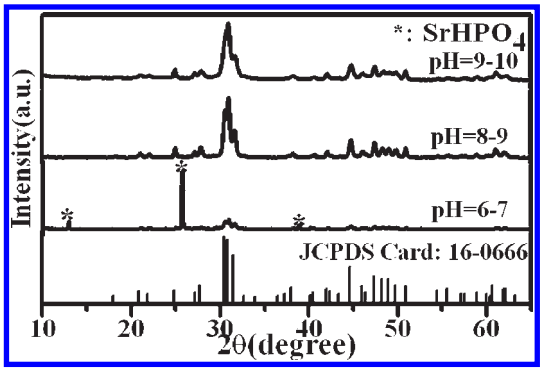

Figure 3. XRD patterns of the nanocrystalline chloroapatite samples prepared at different pH values.

Figure 3 shows the XRD patterns of the $Sr_5(PO_4)_3Cl$:Eu^{2+} powders synthesized at 180 °C for 24 h at different pH values. For the samples prepared with pH 6—7, both $SrHPO_4$ and $Sr_5(PO_4)_3Cl$:Eu^{2+} phases appeared. When the samples were prepared with pH 8—10, the XRD peaks can be well indexed to the standard JCPDS card (16−0666) with hexagonal phase (space group $P63/m$).

Figure 4 gives the FT-IR spectra of the nanorods and bulk material. There is no significant difference between their spectra, indicating that no EDTA remains on the surface of the nanorods. The 459 cm^{-1} band is assigned to the ν_2 phosphate mode. The bands at 559 and 592 cm^{-1} derive from the ν_4 bending vibration of P−O mode and the 950 cm^{-1} band results from the ν_1 symmetric P−O stretching vibration. The strong bands at 1026 and 1072 cm^{-1} are due to the triply degenerate ν_3 antisymmetric P−O stretching vibration of the PO_4^{3-} groups.[18] The bands centered at about 1630 and 3432 cm^{-1} can be due to the water adsorbed on the surface of the samples. Generally, the band corresponding to the O−H stretching mode in hydroxyapatites appears as a narrow peak at about 3570 cm^{-1}.[19] No narrow peak was observed in the similar region, revealing the formation of high purity $Sr_5(PO_4)_3Cl$:Eu^{2+}.

Morphology. Panels a and b of Figure 5 show the SEM images of the $Sr_5(PO_4)_3Cl$:Eu^{2+} products obtained with

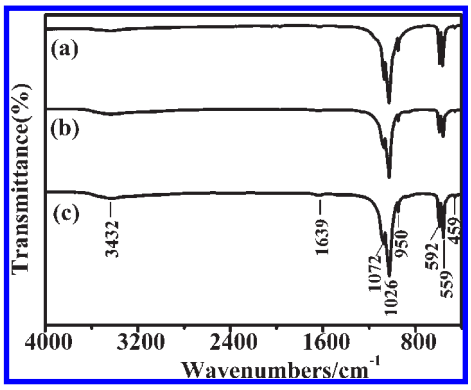

Figure 4. FT-IR spectra of Eu^{2+}-doped $Sr_5(PO_4)_3Cl$. (a) Bulk $Sr_5(PO_4)_3Cl$; (b, c) nanorods synthesized with and without EDTA.

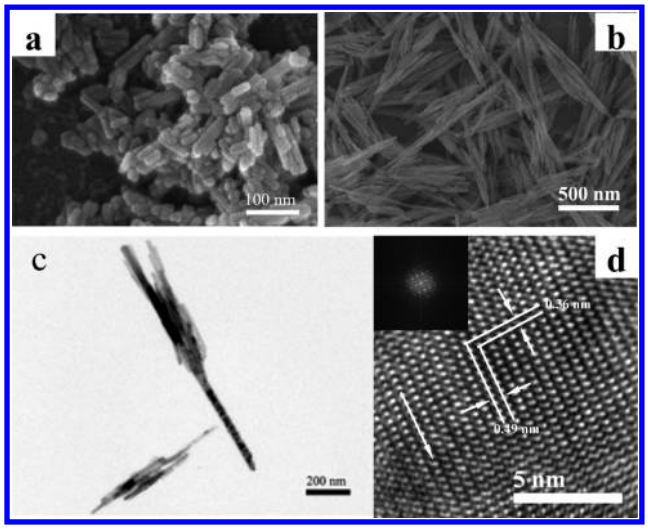

Figure 5. Typical SEM images of the $Sr_5(PO_4)_3Cl$:Eu^{2+} products obtained in the absence of EDTA (a) and in the presence of 0.50 g of EDTA (b). TEM (c) and HRTEM (d) images and its corresponding FFT pattern (inset) taken from the tip of an individual nanorod.

and without EDTA, respectively. The $Sr_5(PO_4)_3Cl$:Eu^{2+} product obtained without EDTA exhibits a non-uniform distribution, and agglomeration to some extent by nanorods with the size of about 100 nm in length and 20 nm in width. In the presence of 0.5 g of EDTA, the products are composed of uniform nanorod bundles which are around 200 nm in diameter and 800 nm in length. The nanorod bundles consist of parallel nanorods with diameters ranging from 20 to 30 nm (Figure 5b). The EDS spectrum (Figure 2) reveals no impurities, confirming the high purity of these nanorod bundles. In addition, the relative molar ratio of Sr/P is about 1.66, which matches well with the theoretic value.

To further understand the fine structure of the nanorods and estimate the grow direction, TEM and HRTEM studies of the $Sr_5(PO_4)_3Cl$:Eu^{2+} sample obtained at 180 °C for 24 h with 0.5 g of EDTA are employed (Figure 5c,d). The TEM image shows the same nanorod bundles as the SEM represent (Figure 5b). The HRTEM image clearly shows lattice fringes with interplanar spacing of 0.49 and 0.36 nm that correspond to the [110] and [002] planes of the hexagonal crystal structure of the $Sr_5(PO_4)_3Cl$ Eu^{2+}, respectively. It indicates that the obtained $Sr_5(PO_4)_3Cl$:Eu^{2+} nanorods are single crystals grown

(18) Fowler, B. O. *Inorg. Chem.* **1974**, *13*, 194.
(19) Tanaka, H.; Yasukawa, A.; Kandori, K.; Ishikawa, T. *Langmuir* **1997**, *13*, 821.

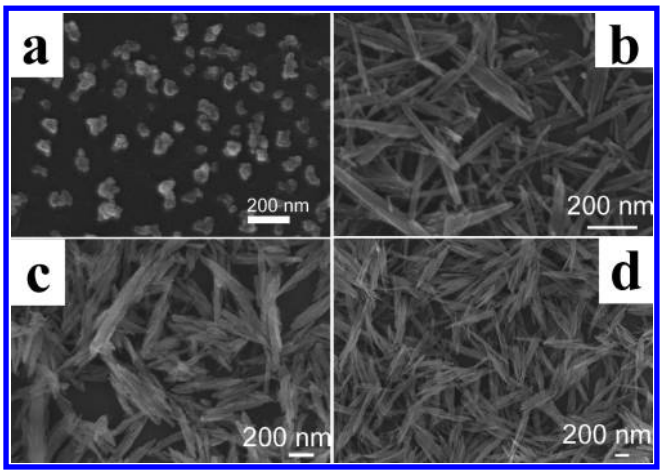

Figure 6. FE-SEM images of $Sr_5(PO_4)_3Cl:Eu^{2+}$ samples at different hydrothermal growing stages: (a) 0.5 h; (b)1.5 h; (c) 2 h; (d) 24 h.

along the [002] direction, the *c*-axis. The corresponding fast Fourier transform (FFT) pattern (inset Figure 5d) further demonstrates that the as-synthesized $Sr_5(PO_4)_3Cl:Eu^{2+}$ nanorod bundles are composed of well-crystallized hexagonal single crystal nanorods.

Formation Mechanism for the $Sr_5(PO_4)_3Cl:Eu^{2+}$ Nanorod Bundles. The growth process of the $Sr_5(PO_4)_3Cl:Eu^{2+}$ nanorod bundles through the hydrothermal method was investigated by observing the images of the $Sr_5(PO_4)_3Cl:Eu^{2+}$ crystals at different stages. Figure 6 shows the FE-SEM images of $Sr_5(PO_4)_3Cl:Eu^{2+}$ samples at different hydrothermal growth stages. The primary particles of $Sr_5(PO_4)_3Cl:Eu^{2+}$ nanoparticles can be seen clearly in Figure 6a for $t = 0.5$ h. When the reaction continued to 1.5 h, the primary particles of $Sr_5(PO_4)_3Cl:Eu^{2+}$ grew as rodlike crystals. Then a long rod may act as a leader crystal in the center of the bundles, and some short rods closely connected parallel to the surface of the leading rod result in the bundle structure formation. After reaction for 24 h, the uniform nanorod bundles formed. On the basis of the experimental results, the formation mechanism for the $Sr_5(PO_4)_3Cl:Eu^{2+}$ nanorod bundles is speculated to be as follows: (1) In the synthetic process, EDTA may act as chelating and capping agent to kinetically control the growth rate of different crystal faces through selective adsorption and desorption.[20] (2) In the first process, the Sr^{2+} ions are chelated by EDTA ligands. When $Sr_5(PO_4)_3Cl:Eu^{2+}$ crystals nucleate from the precursor solution (Stage I), the EDTA is dissociated from the cation ions; it will bind to the specific surface of the precipitated $Sr_5(PO_4)_3Cl:Eu^{2+}$ and slow down the growth speed of the crystal faces. Then, the rodlike $Sr_5(PO_4)_3Cl:Eu^{2+}$ crystal will grow via oriented attachment (Stage II). (3) In the presence of EDTA, a long, large $Sr_5(PO_4)_3Cl:Eu^{2+}$ nanorod undergoing rapid growth may act as a leader crystal in the center of the bundle, while some shorter nanorods will have the tendency to aggregate together, side by side, to form a bundle because of the stronger van der Waals attraction along the long axis of the rods, resulting in a shuttlelike structure (Stage III). With prolonged reaction time, all the Sr^{2+} precursors

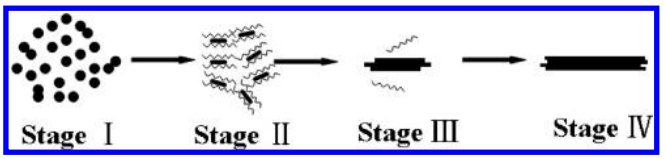

Figure 7. Possible formation mechanism of the $Sr_5(PO_4)_3Cl:Eu^{2+}$ nanorod bundles.

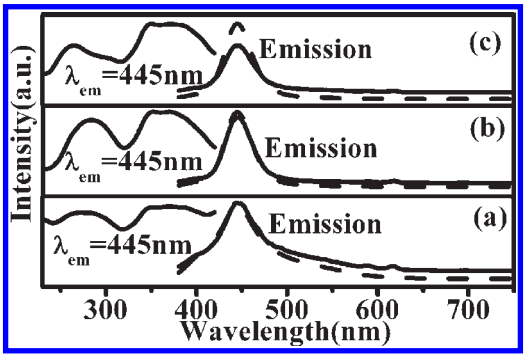

Figure 8. Excitation and emission spectra for the $Sr_5(PO_4)_3Cl:Eu^{2+}$ samples prepared with (a) 1 mL $N_2H_4\cdot H_2O$; (b) 2 mL $N_2H_4\cdot H_2O$; and (c) 4 mL $N_2H_4\cdot H_2O$. (For the emission curves: solid line, $\lambda_{ex} = 275$ nm; dashed line, $\lambda_{ex} = 350$ nm).

from the EDTA-Sr complex are depleted, and the bundles stop growing longer (Stage IV). This is similar to that described in the report of h-WO_3 nanowire growth.[21] The whole process of crystal bundle structure evolution is schematically shown in Figure 7.

Luminescence Properties. Figure 8 presents the excitation and emission spectra of the as-synthesized $Sr_5(PO_4)_3Cl:Eu^{2+}$ nanorods with different amounts of hydrazine hydrate. The excitation spectra exhibit two strong broad bands in the range of 220−420 nm, which is attributed to the typical $4f^7\ (^8S_{7/2}) \rightarrow 4f^6 5d^1$ transition of the Eu^{2+} ions. The emission spectra consist of a strong band at about 445 nm and some weak sharp peaks in the range of 580−630 nm, which are due to the typical $4f^6 5d^1 \rightarrow 4f^7\ (^8S_{7/2})$ transition of the Eu^{2+} ions and the typical $^5D_0 \rightarrow {}^7F_J$ ($J = 1, 2$) transitions of the Eu^{3+} ions, respectively. The intensity of these weak peaks decreased with increasing $N_2H_4\cdot H_2O$ content, revealing that the more $N_2H_4\cdot H_2O$ was added, the more the Eu^{3+} ions were reduced. Therefore, $N_2H_4\cdot H_2O$ plays an important role in the reduction process from the Eu^{3+} to Eu^{2+} ions.

Hydrazine is a powerful strong reductant and has been widely used in various chemical operations.[22] The standard redox potentials of Eu^{3+}/Eu^{2+} and N_2/N_2H_4 are −0.43 V and −1.15 V, respectively. Because of the redox potentials, the Eu^{3+} ions can be easily reduced to Eu^{2+} ions by $N_2H_4\cdot H_2O$. The reaction between Eu^{3+} ions and hydrazine proceeds according to the following equation:

$$N_2H_4\cdot H_2O + 4OH^- + 4Eu^{3+} \rightarrow 4Eu^{2+} + N_2 + 5H_2O \quad (1)$$

So a high pH would accelerate the reaction toward the right to form Eu^{2+} ion. However, if the pH is higher than

(20) Luo, F.; Jia, C. J.; Song, W.; You, L. P.; Yan, C. H. *Cryst. Growth Des.* **2005**, *5*, 137.

(21) Gu, Z. J.; Ma, Y.; Yang, W. S.; Zhang, G. J.; Yao, J. N. *Chem. Commun.* **2005**, 3597.

(22) Peng, Q.; Dong, Y. J.; Li, Y. D. *Inorg. Chem.* **2003**, *42*, 2174.

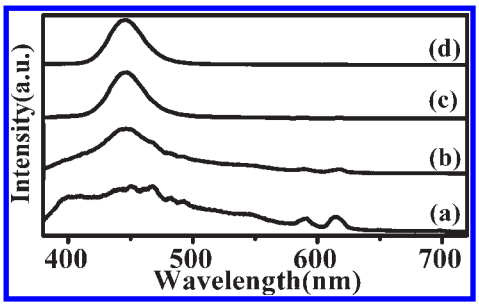

Figure 9. Emission spectra for $Sr_5(PO_4)_3Cl:Eu^{2+}$ samples obtained after hydrothermal treatment at 180 °C for (a) 2 h, (b) 4 h, (c) 6 h, and (d) 12 h.

10, the sample would be more a chloro(hydroxyl)apatite than a pure chloroapatite, and the existence of OH^- would reduce the luminescent intensity dramatically.[23] The reduction ability of the N_2H_4 was thus limited by the pH.

The reduction from the Eu^{3+} to Eu^{2+} ions was also affected by reaction time (Figure 9). When the reaction time is 2 h, the typical emission of the Eu^{3+} ions at about 614 and 592 nm can be observed clearly. As the reaction time was prolonged, the emission bands of the Eu^{3+} ions became weaker. Meanwhile, the emission band of the Eu^{2+} ions appeared, indicating that the Eu^{3+} ions began to be reduced to Eu^{2+} ions. When the reaction time exceeded 6 h, most Eu^{3+} ions can be reduced to Eu^{2+} ions. The emission intensity of as-obtained $Sr_5(PO_4)_3Cl:Eu^{2+}$ is about 10% lower than that of bulk material. The lower intensity of the nanophosphor was mainly associated with the energy-transfer processes to the surface through adjacent dopant ions, the luminescence quenching of surface dopant ions, and the quenching effect of the defects.[24] Therefore, the further treatment, such as surface modification or condition optimization, will improve the intensity of as-obtained $Sr_5(PO_4)_3Cl:Eu^{2+}$.

Conclusions

In summary, high purity $Sr_5(PO_4)_3Cl:Eu^{2+}$ blue nanophosphors with one-dimensional nanorods and nanorod bundles were successfully synthesized using a mild and facile hydrothermal method. In the presence of EDTA, the $Sr_5(PO_4)_3Cl:Eu^{2+}$ rodlike bundles grow through oriented attachment assisted by a side-by-side self-assembly mechanism. The photoluminescence properties demonstrated that the Eu^{3+} ions were successfully reduced to Eu^{2+} ions through $N_2H_4 \cdot H_2O$. The as-prepared nanophosphors exhibited intense blue emission, which may have potential applications in building mini-optoelectronic devices. More importantly, our new simple synthetic route opens up a new way to prepare other nanoscale phosphors containing divalent europium ions by the aqueous method.

Acknowledgment. This work is financially supported by the National Natural Science Foundation of China (Grant 20771098) and the Fund for Creative Research Groups (Grant 20921002), and the National Basic Research Program of China (973 Program, Grants 2007CB935502 and 2006CB601103).

(23) Maas, H.; Currao, A.; Calzaferri, G. *Angew. Chem., Int. Ed.* **2002**, *41*, 2495.

(24) Abrams, B. L.; Holloway, P. H. *Chem. Rev.* **2004**, *104*, 5783. Sudarsan, V.; van Veggel, F. C. J. M.; Herring, R. A.; Raudsepp, M. *J. Mater. Chem.* **2005**, *15*, 1332. Stouwdam, J. W.; van Veggel, F. C. J. M. *Langmuir* **2004**, *20*, 11763. Kömpe, K.; Borchert, H.; Storz, J.; Lobo, A.; Adam, A.; Möller, T.; Haase, M. *Angew. Chem., Int. Ed.* **2003**, *42*, 5513.